

On drug-base incompatibilities during extrudate manufacture and fused deposition 3D printing

Aim: 3D printing can be applied for point-of-care personalized treatment. This study aimed to determine the manufacturability and characteristics of 3D printed, drug-loaded implants for alcohol misuse. **Materials & methods:** Disulfiram was the drug substance used and polylactic acid (PLA) the base material. Implantable devices were designed *in silico*. Drug and PLA were placed into the extruder to produce a 5% blend at 1.75-mm diameter. Material characterization included differential scanning calorimetry, thermogravimetric analysis plus inverse GC-surface energy analyzer. **Results:** Implantable constructs from the PLA feedstock were acquired. The extrusion processes had a detrimental effect on the active pharmaceutical ingredient-base blend. differential scanning calorimetry and thermogravimetric analysis analysis indicated drug-base interactions. Thermal history was found to influence inverse GC probe interaction. **Conclusion:** Drug-base incompatibilities must be considered during 3D printing.

First draft submitted: 9 September 2016; Accepted for publication: 17 October 2016; Published online: TBC

Keywords: 3D printing • active • alcohol misuse • disulfiram • incompatibilities • materials characterization • polylactic acid

The ability to design and manufacture pharmaceutical dosage forms that are tailored specifically for the patient is becoming increasingly important within the field of healthcare [1]. Personalized medicine offers the service provider with scope to customize treatment regimens based upon unique underlying genetic profiles. That is to say, variations in patient physiology, disease severity, drug responsiveness and side effect presentation may all be accounted for to permit optimal dosing schedules and attain effective disease management [2]. Clearly, this approach represents a paradigm shift from the 'one size fits all' strategy currently employed within modern day healthcare.

Recent developments within the field of pharmaceutical technology have provided innovative and evermore tangible methods to deliver personalized medicine to mem-

bers of the community; prime examples include ink-jet arrays [3] and 3D printing platforms [4]. As a result of the constantly decreasing size and cost of the units, potential now exists to offer individualized services at the point-of-care. Appropriate sites for such service provision would include outpatient clinics within the secondary care setting or community pharmacy premises. Within such locations, the fabrication of a personalized dosage form could feasibly arise in response to a legally valid prescription containing predefined patient details. Here, the healthcare provider (e.g., a pharmacist) could manufacture a variety of dosage forms including tablets [5], oro-dispersible wafers [3], suppositories and importantly for the work presented herein implantable devices for subsequent professional administration [2].

Michael J Davies^{1*}, Emily Costley¹, James Ren¹, Paul Gibbons¹, Anett Kondor² & Majid Naderi²

¹The School of Pharmacy & Biomolecular Sciences, Liverpool John Moores University, Liverpool, L3 3AF, UK

²Surface Measurement Systems, Unit 5, Wharfside, Rosemont Road, Alporton, London, HA0 4PE, UK

*Author for correspondence:

Tel.: +44 151 231 2024

Fax: +44 151 231 2170

m.davies1@ljmu.ac.uk

Implantable dosage forms allow for the delivery of active pharmaceutical ingredients (APIs) to the body over an extended period of time [6]; typical agents for delivery include contraceptives and hormone replacement therapies. Such formulations confer a number of advantages to the user including the precise and steady release of API to achieve consistent plasma levels plus improved compliance with prescribed regimens and the ability to continue with life as normal. To date, limited consideration has been given to the formulation of implantable devices for personalized medicine regimens and in this regard we believe that 3D printing technology would lend itself well.

The process of 3D printing involves the accurate, layered deposition of a material to form a predetermined solid object [7]. Traditionally, the approach has been employed to produce a range of nonmedical plastic, metallic and ceramic architectures. However, more recently interest has been stimulated in this approach to support the field of healthcare [8].

This trend may be ascribed to several factors including the exact control over construct arrangement, the capacity to control drug release profiles and the capability to personalize the dosage form to support patient needs [9]. A number of 3D printer subgroups are available to manufacture formulator-defined solid constructs; for instance, selective laser sintering [10], thermal inkjet [3] and of interest herein fused deposition modeling (FDM) [4]. The latter strategy relies upon the synthesis of an *in silico* file that guides the trajectory of a heated, thermoplastic extrusion head in the x-y plane. The melted extrudate is deposited in a layer-like fashion with depth in the construct being achieved via movement of the baseplate in the z-plane [5]. As the material cools it hardens to the solid state, which may then be suitable for direct patient end use to support individualized disease management.

A number of polymers are currently available for use as base materials to support FDM. For example, polycaprolactone (PCL) and polyvinyl alcohol (PVA) may be applied to provide drug release over a period of hours [11], while polylactic acid (PLA) can offer the formulator release characteristics spanning days [2]. For illustration, in 2015 Goyanes and coworkers considered the suitability of PVA in controlling the release rate of aminosalicylate from tablets produced by FDM [11]. Here, an API saturated ethanol solution was prepared in which a PVA filament was immersed for 24 h. On drying, the group successfully produced tablets with predetermined dimensions and characterized the drug release profiles. This work underscored the fact that FDM offers healthcare providers a cheap and flexible way in which to produce dosage forms with variable infill percentages. Furthermore, in 2015

Water and colleagues considered the application of PLA as the base filament for nitrofurantoin-loaded dosage forms [2]. Here, a microcompounder was used to incorporate PLA and nitrofurantoin. The blend was subsequently recirculated and extruded to support dosage form production. In a similar fashion to Goyanes and coworkers, this work highlighted the clear potential for 3D printing in the field of healthcare.

Sorption methods can be utilized to probe material characteristics in order to predict behavior during manufacture and patient end use; such approaches may either be dynamic or static. Standard procedures such as the determination of the surface area by nitrogen adsorption at 77 K are based on the latter. In recent years, sorption methods have become increasingly important since they provide several advantages over standard static techniques; including for example probe molecules can be chosen with chemical properties that are appropriate or relevant to the information required or problem to be addressed and may be site specific; vapor phase molecular probes are extremely sensitive probes for determining the surface chemistry at submonolayer coverages for particulate materials and typically, both kinetic and equilibrium thermodynamic data can be obtained using molecular probe techniques [12].

For a sorption measurement, a carrier gas is used (instead of performed under vacuum) to transport the probe molecule (adsorptive) to the material under investigation (adsorbent). This allows faster equilibration under these experimental conditions. The most common sorption techniques are gravimetric methods and inverse GC (iGC). The iGC platform exchanges the roles of the phases in classical GC whereby the adsorbent under investigation is placed into a column while a known adsorptive is used in the gas phase. As in analytical GC, the retention time is obtained as the fundamental parameter measured. The retention time can be converted into a retention volume, which is directly related to several physicochemical properties of the solid (i.e., adsorbent). These properties can be thermodynamic parameters, such as surface energy or heat of sorption and kinetic parameters, such as the diffusion constant and the activation energy of diffusion. It is also possible to determine the uptake for both physisorption and chemisorption processes. In the first case, a sorption isotherm is obtained, which allows the computation of the surface area and heterogeneity profiles. In the latter case the amount adsorbed is much higher than the amount desorbed and a titration method is designed to calculate the amount irreversibly chemisorbed onto a surface. Apart from its high versatility and speed, the main benefit of iGC is its sensitivity at the surface of the sample. Unlike most other sorp-

tion techniques, iGC allows an accurate measurement at extremely low partial pressures. This makes iGC a valid tool in the determination of thermodynamic properties. It can operate in the Henry range (linear portion of the isotherm) where only high-energy sites are accessed by the probe molecule and there is no probe molecule-probe molecule interaction. The interaction with the high-energy sites allows the detection of very small differences between materials. For this reason, iGC has been used successfully in various cases for the investigation of batch-to-batch problems.

Based on a unique injection mechanism, the iGC surface energy analyzer (SEA) provides major improvement in the injection pulse sizes allowing the BET region of the isotherm to be obtained; the approach has been applied to the work presented herein. The iGC SEA provides an unrivalled injection ratio of 1–4000, as compared with 1–60 of the iGC. If the surface area of the sample is provided, the iGC SEA can be automatically programmed to inject the precise amount of probe vapor in order to achieve different user defined surface coverages. The measurement of surface properties at different surface coverages will result in a surface heterogeneity profile of the sample. The understanding of energy distributions is particularly useful at interface boundaries of formulations, as well as to distinguish subtle differences in the surface chemistry of samples that may be used as either actives or base materials in disease management.

Alcohol dependence may be described as the physical or psychological obligation for an individual to consume alcohol-containing beverages [13]. The issue is of growing concern in the developed world. For example, alcohol misuse was recorded as the second highest cause for hospital admissions within the UK in 2013–2014 [14]. Alcohol dependence may lead to acute and chronic health complications plus place significant strain upon healthcare systems. In the case of the former, individuals may regularly experience depression, anxiety and suffer mild-to-severe trauma [15]. Over the longer term there is an increased likelihood for the development of cancer, liver disease and the potential for psychological issues to present [16].

Current UK guidelines state that the pattern and severity of alcohol misuse should be initially investigated on an individual patient basis [17]. Here, the aim should be for complete abstinence with the support of an assisted withdrawal program. Detail of the approach is beyond the remit of this study, however a number of therapeutic interventions can be made to help sustain total abstinence. Within the UK, disulfiram is prescribed to manage alcohol dependence [18]. This agent inhibits the action of acetaldehyde dehydrogenase that is responsible for metabolizing alcohol on delivery to

the body. The resulting effect leads to an increased concentration of acetaldehyde that causes flushing, increased body temperature and vomiting [19]. Such responses intend to deter the patient from consuming alcohol. Here, the patient must be fully compliant with medical guidance in order to attain the desired treatment outcome (i.e., alcohol abstinence). Thus, a key drawback with the approach is that the patient may consciously decide not to administer the API on a daily basis. One possible route to circumvent this treatment-limiting drawback would be to deliver the API as an implantable device.

This study aims to fabricate disulfiram-containing implants via FDM 3D printing and evaluate resulting material properties. Here, we have chosen PLA as the model base material for study as it is biodegradable and biocompatible plus it may facilitate controlled drug release over hours when delivered to the body [2]. Within this work we shall offer comment upon the feasibility of the approach/use of materials, or not, for chronic disease management at the point-of-care.

Materials & methods

Materials

A PLA filament spool, of 1.75 ± 0.05 mm diameter, was purchased from Wanhao Inc. (FL, USA; BN: 201505051508003). Disulfiram of 97% purity was acquired from Acros Organics (NJ, USA; BN: A0146315); the chemical structure of the compound is presented in [Figure 1](#). During this work, ScotchBlue professional tape was used as the surface on which to print.

Methods

Preparation of the disulfiram-PLA filament

Initially, 280 g of PLA feedstock was cut into small fragments of approximately 1–2 cm in length. The material was subsequently placed into an oven set at 60°C for 2 h to remove adsorbed moisture. Appropriate amounts of API and base were taken and weighed using a five-place analytical balance (A&D, BM-252; CA, USA) so as to satisfy a 5% PLA-disulfiram blend. In addition, a sample of the preconditioned PLA was taken for use as the placebo. The API and base materials were gradually fed into a Noztek Pro filament extruder (West Sussex, UK) to allow for mixing and drug-loaded filament production. With respect to the 5% PLA-disulfiram blend, one batch was extruded at 140°C and the other at 170°C. The control sample was extruded at 170°C, with one recirculation phase through the extruder unit. In order to ensure uniform mixing the API-containing extrudate was recycled through the extruder a further time. Upon completion, the filaments were stored in a vacuum desiccator

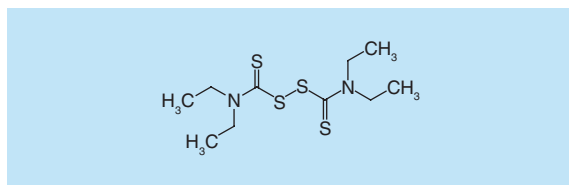


Figure 1. Disulfiram.

until required for printing in order to guard against moisture adsorption.

Implant printing

The constructs were generated using the Wanhao Duplicator 4 Desktop 3D printer (Wanhao Inc., FL, USA). The architecture of each dosage form was defined using the SolidWorks® Education Edition 2015–2016 SP3.0 software platform (Dassault Systemes, France). In order to prepare the design files for 3D printing MakerWare 2.2 software was employed (NY, USA). The implant dimensions were fixed at 40 mm in length and 3 mm in diameter so as to reflect the dimensions of commercially available implantable products [20]. A rendered image of the implant device devised for this work is shown in **Figure 2**.

Throughout the design and manufacturing process various parameters were selected for product optimization. For example, prior to fabrication, features such as standard PLA resolution, building plate temperature of 20°C, layer height of 200 µm, extrusion temperature of 210°C, extrusion speed of 90 mm/s and travel speed of 150 mm/s and infill percentage of 100% were confirmed within the software packages. In total, ten implants were printed using the native PLA feedstock and a further ten were printed using extruded PLA.

Material characterization

Determination of filament morphology

Samples of the PLA feedstock, extruded PLA, 5% PLA-disulfiram blend extruded at 140°C and 5% PLA-disulfiram blend extruded at 170°C were measured using a digital calliper. In order to quantitatively assess variability along a fixed length of the filaments, a 5 cm sample was taken and the width was recorded at 1



Figure 2. A rendered image of the implant of fixed dimensions 40 mm length and 3 mm diameter.

cm intervals. In addition, photographs of the filaments were taken using a Nikon D60 digital single lens reflex camera (Nikon, Japan) with the macro mode selected.

Determination of implant morphology & mass

Dimensions of the implants were measured using a digital calliper. The mass of each implant produced was determined by a 5-place analytical balance (AND, BM-252; CA, USA). Once again, images of the gross structures were collected using a Nikon D60 digital single lens reflex camera (Nikon, Japan) with the macro mode selected.

Scanning electron microscopy

Scanning electron microscopy (SEM) (Quanta 200 SEM, FEI, Holland) was utilized to visualize the gross morphology of the filaments and the implants. Here, the samples were dried and placed on double sided carbon tape ready for coating. Thereafter the samples were coated at 25 milliamps, approximately 15 nm coat, in a K550X sputter coater (Emitech, UK) with palladium in an argon atmosphere. Subsequently, the material was scanned using an acceleration voltage of 10 kV at a working distance of approximately 10 mm.

Thermal analysis of filaments & implants

Differential scanning calorimetry

A Perkin Elmer DSC7 (WA, USA) was employed to perform the thermal analysis. An average sample mass of 5.85 mg was taken for the native disulfiram, PLA feedstock, extruded PLA, 5% PLA-disulfiram blend extruded at 140°C, 5% PLA-disulfiram blend extruded at 170°C, implant printed from the PLA feedstock and the implant printed from the extruded PLA. In each case, the samples were placed directly into a Perkin Elmer aluminium pan (Shelton, USA; BN: 02190041) prior to analysis. Nitrogen was used as the purge gas (20 ml/min) and the heating rate was 10°C/min starting at room temperature (e.g., 25°C). The data were collected and analyzed using Pyris Series software (v 3.80).

Thermogravimetric analysis

A TGA Q50 (TA instruments) was employed to conduct further thermal analysis. An average mass of 14 mg of disulfiram, PLA feedstock, extruded PLA, 5% PLA-disulfiram blend extruded at 140°C, 5% PLA-disulfiram blend extruded at 170°C, implant printed from the PLA feedstock and the implant printed from the extruded PLA were placed into a platinum pan. Nitrogen was used as a purge gas with a balance flow rate of 40 ml/min and sample flow rate of 60 ml/min, the heating rate was 10°C/min starting at room temperature (e.g., 25°C) and the mode was TGA 1000 in a ramp format. Data were collected using QSeries

(Q50–1145 = TGA Q50) and analyzed using Universal Analysis 2000 software (v 4.5A). The settings were modified slightly to conduct the thermal analysis of disulfiram to investigate the effect of exposure to temperatures of 170°C for 30 min. Here, all parameters remained constant, however the mode was TGA 1000 in a heat and hold format.

iGC analysis

All analyses were carried out using iGC-SSEA [21]. The data were analyzed using both standard and advanced SEA Analysis Software (Cirrus Plus Analysis Software, v.1.2.1). Approximately 100–170 mg of the samples were packed into individual iGC silanized glass column, and was run at a series of surface coverage with alkanes and polar probe molecules to determine the dispersive surface energy (γ_s^D) as well as the acid-base free energy of adsorption (ΔG_{sp}). In this study, the sample column was preconditioned for 2 h at 30°C and 0% RH with 10 ml/min helium carrier gas. The experiment was conducted at 30°C with 10 ml/min total flow rate of helium, and using methane for dead volume corrections.

Results

Material visualization

At the outset, variable blends of the base material/API were obtained or extruded to form single filament strands (Figures 3A–D). Subsequently, the PLA feedstock strand (Figure 3A) and the extruded PLA strand (Figure 3B) were loaded into the FDM 3D printer to produce implantable devices (Figure 3E & F).

The native PLA feedstock (Figure 3A) and extruded PLA (Figure 3B) presented as white, single filament strands that were able to pass through the head of the FDM 3D printer. On inspection, the extruded PLA was thinner and appeared to demonstrate numerous undulations across the entire length. On the introduction and subsequent blending of disulfiram at 140°C, the filament became discolored and nonuniform (Figure 3C). This observation was more apparent when the material was extruded at the higher operating temperature of 170°C (Figure 3D). Here, the outer surface was darker and more irregular in shape. With regard to the implant devices, the dosage form produced using the PLA feedstock presented as a smooth construct (Figure 3E), while the implant produced from the extruded PLA exhibited distinct layers plus a number of structural defects (Figure 3F).

Filament & implant analysis

In order to investigate the cross-sectional uniformity of the PLA feedstock/extruded filaments digital calliper measurements were taken. Here, a representative

sample of 5 cm length of each material was examined and measurements were recorded at 1 cm intervals. The data were averaged and recorded in Table 1.

The data presented in Table 1 are supportive of the visual inspections presented above. That is to say, the cross-sectional uniformity of the filaments varied according to the conditions the material was exposed to. As anticipated, the native PLA feedstock demonstrated minimal variation over the 5 cm sample length. However, on extrusion the variation increased as demonstrated by the larger SD presented in Table 1. Once the drug was incorporated into the blend, the variation increased further and the 5% PLA-disulfiram blend extruded at 140°C resulted in an increased diameter by 0.72 mm than that of the extruded PLA with a three-times greater variation along the sample length. The 5% PLA-disulfiram blend extruded at 170°C resulted in even greater variation.

On extrusion, this blend was very inconsistent with parts in liquid form and others congregating at the extruder exit in thick bulbous structures. Further to this, when the 5% PLA-disulfiram filament was being extruded at 170°C a noticeable, unpleasant odor was produced suggesting the release of sulfur from degradation of the API (Figure 1). Subsequently, the mass and measurements of the 3D printed implants were investigated; the data are presented in Table 2.

The implants produced using extruded PLA were of lower mass, width, length and volume and generally demonstrated greater variation in these terms when compared to those generated from the native PLA feedstock. As a result of the thinner extrudate diameter (e.g., 1.70 mm ave, as per Table 1) gentle force was required to encourage feed through the FDM 3D printer head. This was so because the rotating feeder heads could not fully grip the extrudate to move it toward the heated printer nozzle. Naturally, such undesirable intervention would have contributed to the varied deposition of layers thus leading to greater variety in mass, width, length and volume measurements. In terms of width and length, the variation within the batches was similar for both PLA feedstock and extruded PLA. Implants printed using the extruded PLA were consistently lighter and smaller than those produced from the PLA feedstock.

SEM analysis of filament & implant morphology

A selection of SEM images demonstrating the gross morphology of the disulfiram starting material plus the 3D PLA/extruded filaments and implants are presented in Figures 4 & 5, respectively.

The disulfiram starting material was pellet based, formed from the cohesion of numerous drug-containing microgranules. On observation, a number of gran-

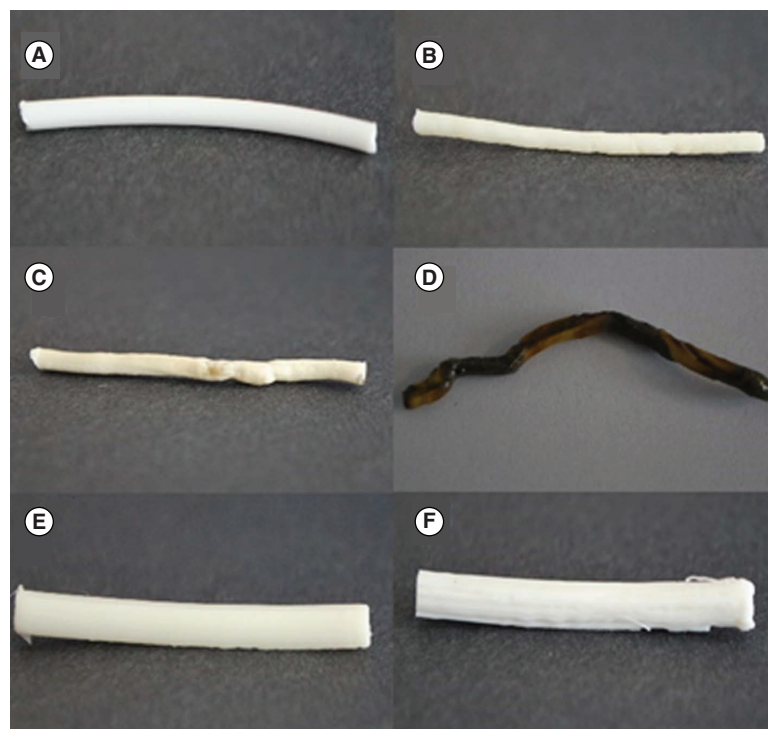


Figure 3. Images of the filaments and implant devices. (A) Poly(lactic acid) (PLA) feedstock, (B) extruded PLA, (C) 5% PLA–disulfiram blend extruded at 140°C (D) 5% PLA–disulfiram blend extruded at 170°C, (E) implant 3D printed using the PLA feedstock and (F) implant 3D printed using the extruded PLA.

ules are distributed over the supporting base which will have sloughed from the main pellet as a result of weak, nonspecific interparticulate forces.

SEM images of the PLA feedstock illustrate a smooth surface of the filament (Figure 5A). However, upon extrusion the surface appeared to become more irregular with a rougher surface (Figure 5B). As the drug was incorporated into the blend at the lower operating temperature of 140°C, there was an increase in surface roughness (Figure 5C). Furthermore, the irregularity in the filament also became more obvious. Once the temperature was increased to 170°C, the filament surface became considerably smoother however the asymmetrical nature of the strand was more prominent (Figure 5D). The images of the implants clearly show the layers that have deposited by the 3D printer in order to produce the construct. The layers forming

the implant from the PLA feedstock (Figure 5E) appear much sharper and more consistent than those from the extruded strand of PLA (Figure 5F).

Thermal analysis

The API along with all of the prepared samples were characterized by thermal analysis. Differential scanning calorimetry (DSC) data indicate that disulfiram melts at 72.2°C, with no observable exo- or endothermic events prior to this temperature. The thermogravimetric analysis (TGA) suggested a 17% weight loss following a 30 min isothermal run at the extrusion temperature of 170°C, as detailed in Figure 6.

Furthermore, a noisy baseline in the DSC data following the PLA melt in the 5% PLA–disulfiram blend extruded at 170°C was noted, as detailed in Figure 8. This point was not observed with other samples. Thus, the data are indicative of the fact that disulfiram degrades upon exposure to high temperatures over an extended period of time.

The filaments and implants, with or without disulfiram, all displayed similar cycles. A single glass transition event occurred at 57.8°C (±4.0°C) and a single melting point displayed at 166.4°C (±2.7°C), which corresponds to previously reported figures [22]. The glass transition point of the PLA feedstock in comparison to the other samples, which had undergone oven drying followed by extrusion, was much more defined. This suggesting that PLA becomes more amorphous once it has been exposed to heat. An exothermic event was displayed between the temperatures of 88.9°C and 106.7°C on all cycles, which could potentially relate to the rearrangement of the polymer chains within PLA matrix. The 5% PLA–disulfiram blends extruded at 140°C and 170°C showed no evidence of the drug melt at 72.2°C, but the PLA melt at 166°C was still present. TGA data showed no significant mass loss therefore it can be inferred that disulfiram is dispersed in PLA as a solid solution.

On DSC analysis, the native PLA feedstock displayed a number of exothermic and endothermic transitions, as detailed in Figure 7. However, once the material had been extruded only a small glass transition point, a single exothermic event and a melt were identified. In this case, the thermal transitions are less

Table 1. Measured properties of the filaments (5 cm length).

Sample	Average diameter ± SD (mm)
PLA feedstock	1.72 (±0.01)
Extruded PLA	1.70 (±0.07)
5% PLA–disulfiram 140°C	2.42 (±0.21)
5% PLA–disulfiram 170°C	1.95 (±0.37)

Table 2. Measured properties of the implants (n = 10).

Source	Average mass \pm SD (mg)	Average width \pm SD (mm)	Average length \pm SD (mm)	Average volume \pm SD (mm ³)
PLA feedstock	343.78 (\pm 16.36)	3.34 (\pm 0.11)	38.17 (\pm 0.21)	334.12 (\pm 22.01)
Extruded PLA	306.87 (\pm 39.98)	3.15 (\pm 0.15)	37.89 (\pm 0.20)	296.47 (\pm 29.03)

PLA: Polylactic acid.

defined in their presentation. Further to this, DSC analysis was conducted on the extruded PLA plus the 5% PLA–disulfiram blends extruded at 140 and 170°C, typical results are illustrated in Figure 8.

The incorporation of disulfiram within PLA further changes the transitional behavior of the polymer. As noted previously, a glass transition stage is visible along with the exothermic event and the melt. However, the trace is not as smooth as the plot detailing the absence of drug. The exothermic event noted in the case of the blend extruded at 170°C has a lower enthalpy of crystallisation (e.g., 1.632 J/g) when compared to the extruded filament without disulfiram and when extruded at 140°C, 6.439 and 7.586 J/g respectively. Furthermore, the enthalpy of the melt is much larger when extruded at 170°C with a value of 25.460 J/g in comparison to the extruded without drug, 5.597 J/g and when extruded at 140°C, 14.080 J/g. In addition to this, the 3D printing process also resulted in differences in the behavior of the polymer, as demonstrated in Figure 9.

Upon inspection of the data presented in Figure 9, it is evident that the glass transition peak occurs at a slightly lower temperature of 58°C once the material has been passed through the 3D printer. In addition, the exothermic event for the material occurs at the higher temperature of 106°C. This is the highest temperature of which the exothermic event was observed for all six samples. Moreover, the trace is smoother with less transitions presenting when compared with the native material.

iGC: surface energy analysis

Surface energy is known to be associated with the chemical composition and the level of crystallization of a sample of interest [23]. This parameter may influence the reaction(s) of a material within different environments, which is important for implantable devices. One relevant area of study is the surface energy profile of a material (i.e., drug-loaded feedstock) in different environments with different processing parameters, in particular the thermal history.

Here, we considered two samples acquired under different processing conditions. One specimen is an extruded 140°C PLA–drug blend with normal air cooling (i.e., designated as PLA + drug noncooled),

the other is an extruded 140°C PLA–drug mix with faster cooling in ice water (designated as PLA + drug cooled). The data presented in Figure 10A outline the dispersive energy profile of the materials as function of surface coverage. Upon inspection, there is no major difference in the dispersive energy term between each sample. Based on the van Oss approach [24], the specific surface energies (γ_s^{AB}) of the samples were calculated using a pair of monofunctional acidic and basic probe molecules (i.e., chloroform – γ_+ : 1.27 mJ/m² and ethyl acetate – γ_- : 475.67 mJ/m²) and the Della Volpe scale was employed. The information presented in Figure 10B confirms that there are stronger variations between the two samples, but in general the difference between the two sets of data on specific energy is not significant.

The iGC–SEA data acquired with different solvents are significantly different as shown in Figure 11A & B. The specific (acid–base) Gibbs free energy of adsorption ΔG_{sp} changes with surface coverage, indicating the heterogeneous nature of the samples. The ΔG_{sp} profiles reflect the interactions with all four polar probe molecules. Higher ΔG_{sp} values can be attributed to a higher concentration of polar surface groups or

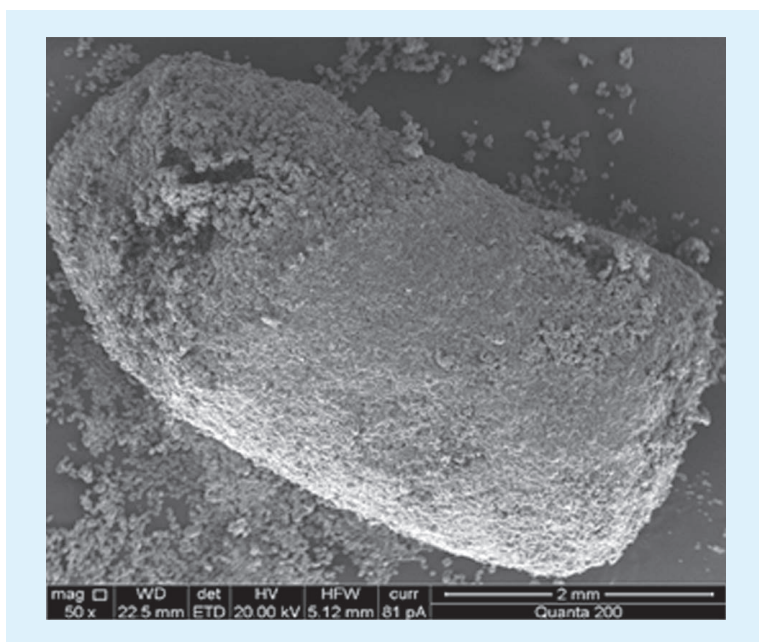


Figure 4. Scanning electron microscopy image of a disulfiram aggregate.

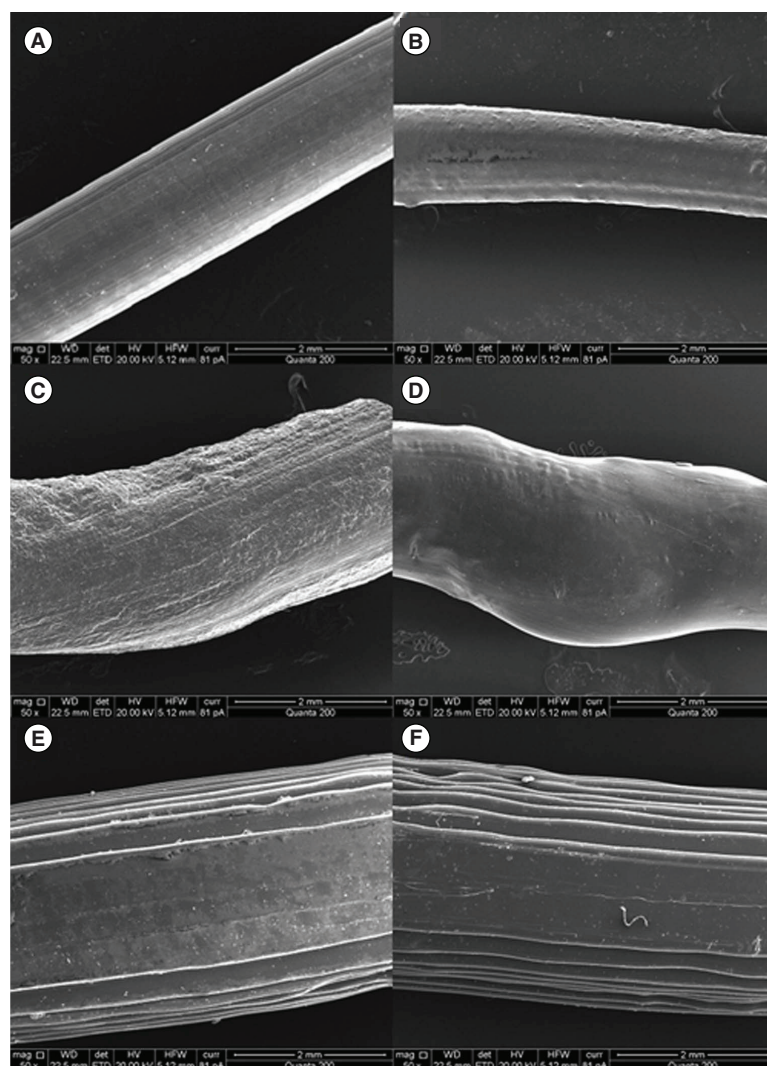


Figure 5. Scanning electron microscopy images of the filaments and implant devices. (A) Polylactic acid (PLA feedstock), (B) extruded PLA, (C) 5% PLA-disulfiram blend extruded at 140°C, (D) 5% PLA-disulfiram blend extruded at 170°C, (E) implant 3D printed using the PLA feedstock and (F) implant 3D printed using the extruded PLA.

different surface groups with higher specific surface energy. As shown in Figure 11A & B, all samples show strong degree of interactions with all polar probes. The surface chemistry of the samples was assessed using the Gutmann acid (K_a) and base (K_b) numbers, determined based on the Gutmann approach [25] using the following polar probes: dichloromethane, ethyl acetate and chloroform. The K_a and K_b values of the samples were calculated using the ΔG_{sp} values of polar probes at 0.01 surface coverage and the results are presented in Figure 12. The K_a/K_b ratio provides an empirical basis for classification of surface with respect to acidity–basicity. It is so called surface specific character (Sc). If the ratio is $Sc > 1$ the surface is considered to be acidic (i.e., electron acceptor ability prevails over electron donor capacity). A $Sc < 1$ shows basic character

whereas $Sc \approx 1$ is the characteristic of amphoteric surfaces.

The surface of the samples show different acid–base character. The noncooled sample is less basic in nature than the cooled sample, having lower basic constant. The clear differences observed between the two samples suggest that the thermal history of the drug-loaded feed is an important variable to be controlled for this particular application (i.e., implant production).

Discussion

Overview

Significant interest now lies in the field of 3D printing to support the personalized medicine paradigm. The ability to manufacture tailored pharmaceutical formulations at the point-of-care is an exciting and imminent prospect. Such development may be ascribed to recent advances in both engineering technology (i.e., FDM) and a more detailed understanding of patient pharmacogenomics. Clearly, in order for the strategy to be effective it is imperative to fully understand the interactions between the API(s) of interest and base material(s) and their related manufacturability. To this end, the present study has considered the feasibility of producing API-loaded PLA implants via FDM with related materials characterization. Key recommendations are provided here in order to support future progression within this discipline of pharmaceuticals.

Exemplar study

Our current study is based upon that conducted by Water and colleagues in 2015, who effectively loaded a PLA filament with nitrofurantoin to produce a custom feedstock suitable for 3D printing [2]. During the work, the group successfully prepared matrix concentrations of 10, 20 and 30% nitrofurantoin. Subsequently, the appropriately weighed PLA and API were fed into the extruder screw channel and underwent 2 min of recirculation before being ejected as a single strand with an average diameter 1.6 ± 0.1 mm. The constructs were designed as disks with predetermined dimensions of 10 mm diameter \times 2 mm depth and were successfully produced via MakerBot Replicator 2 3D printer utilising the custom filament created. Analysis of the construct mass ($n = 3$) indicated that the lower the nitrofurantoin percentage the greater the variation in weight. Furthermore, SEM images of both the extruded filaments and disk constructs confirmed an apparent rougher surface with increased drug loading, which was ascribed to the presence of solid nitrofurantoin within the PLA matrix. This point was further confirmed by x-ray diffraction (XRD) analysis that highlighted nitrofurantoin anhydrate crystals within the disks.

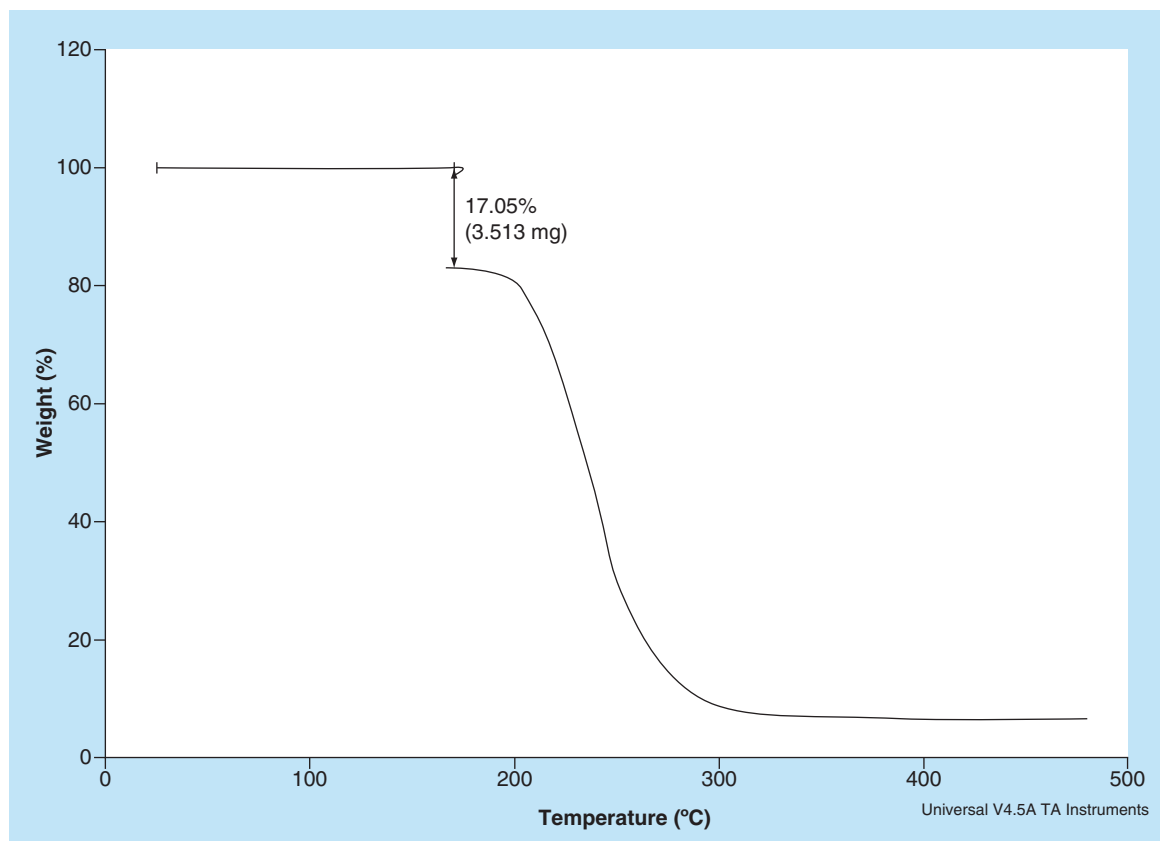


Figure 6. Thermogravimetric analysis data for disulfiram with an isothermal hold at 170°C for 30 min.

Thermal analysis demonstrated a single glass transition event at $56.6 \pm 0.7^\circ\text{C}$, a melting point at $149.6 \pm 0.5^\circ\text{C}$ with no evidence of recrystallization. Due to the absence of a melting point for nitrofurantoin below 235°C , it was inferred that the PLA-nitrofurantoin blend consisted of two immiscible phases. Drug release profiling was conducted over a period of 45 days. Initially, burst release was observed, within the first 3 h, with the highest rate of release for the subsequent 2 days before steadily decreasing over the remaining period. The degree of drug release correlated to the drug loading (i.e., the greater the drug loading, the greater the rate of drug release). Overall, the approach was deemed as a successful way by which to manufacture drug-eluting constructs demonstrating antimicrobial activity.

Material characteristics

Despite applying the approach taken by Water and coworkers, we were unsuccessful in our attempt to manufacture disulfiram-loaded PLA implants to satisfy the personalized medicine paradigm. We attribute the outcome to a number of factors but primarily to API-base incompatibilities at elevated manufacturing temperatures. In order to further the knowledge-base in this sphere of pharmaceuticals, we believe that it is

important to evaluate the processes undertaken, characterize resultant material properties and provide recommendations going forward.

The inherent material incompatibilities led to incongruity in the drug-base filament. This fact in turn resulted in an inability to effectively print because the filament diameter no longer matched the inlet configuration of the 3D printer head. We believe that the diameter of the extruded material is dependent upon a number of factors; primarily the nozzle size dictates the thickness of the produced material, however, base viscoelastic properties also have an influence. The viscoelastic profile of a material is an essential consideration. The resultant swelling of the PLA on release from the extruder nozzle may be influenced by parameters such as screw speed and extrusion temperature. Although the extruded PLA without API was able to be fed through the printer head, the need for application of pressure to encourage the feed led to inconsistencies in the resulting printed implants.

Thermal analysis

Thermal analysis highlighted further issues with the FDM approach. On consideration of the DSC data presented herein, it is clear that an elevation in operat-

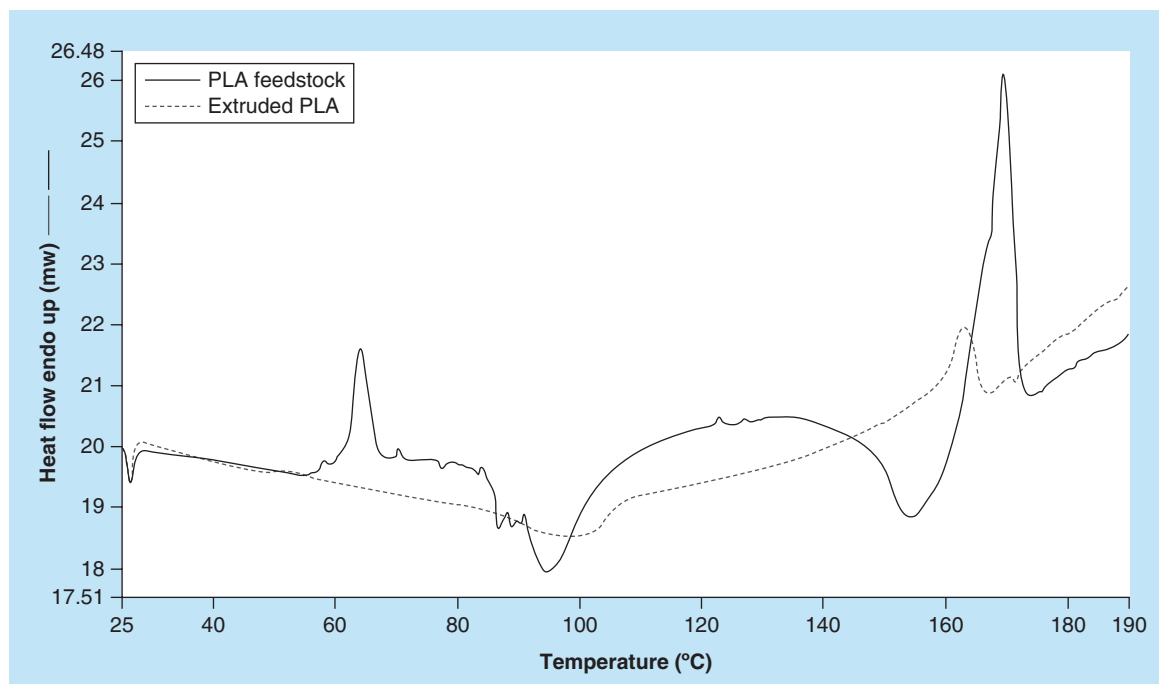


Figure 7. Differential scanning calorimetry plots for polylactic acid feedstock and extruded polylactic acid. PLA: Polylactic acid.

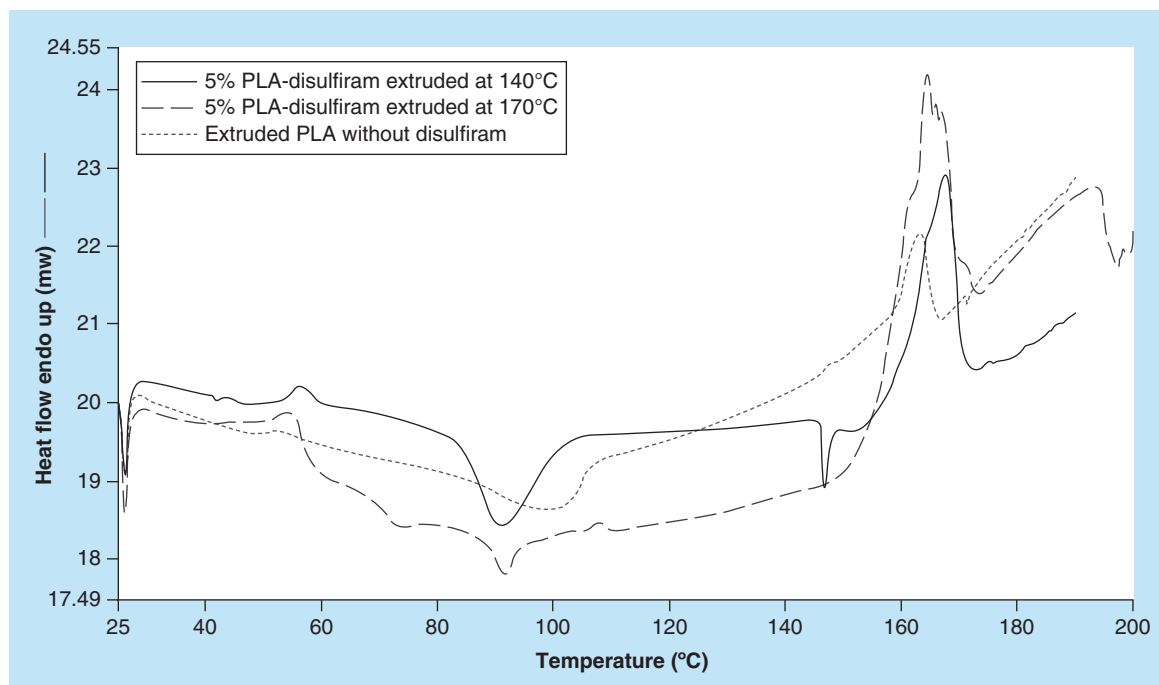


Figure 8. Differential scanning calorimetry plots for extruded polylactic acid and 5% polylactic acid–disulfiram blends extruded at 140 and 170°C. PLA: Polylactic acid.

ing temperature led to the modification of viscoelastic behavior of PLA. Furthermore, processing at a temperature of 170°C caused the API to degrade, a point corroborated by the TGA cycle in Figure 6 and the noisy baseline in Figure 8. However, the TGA cycle of

the API in ramp format did not show as significant a weight loss when compared with the isothermal hold. Thus, we infer that API degrades upon exposure to high temperatures over an extended period. The latter point is central to the feasibility of the FDM

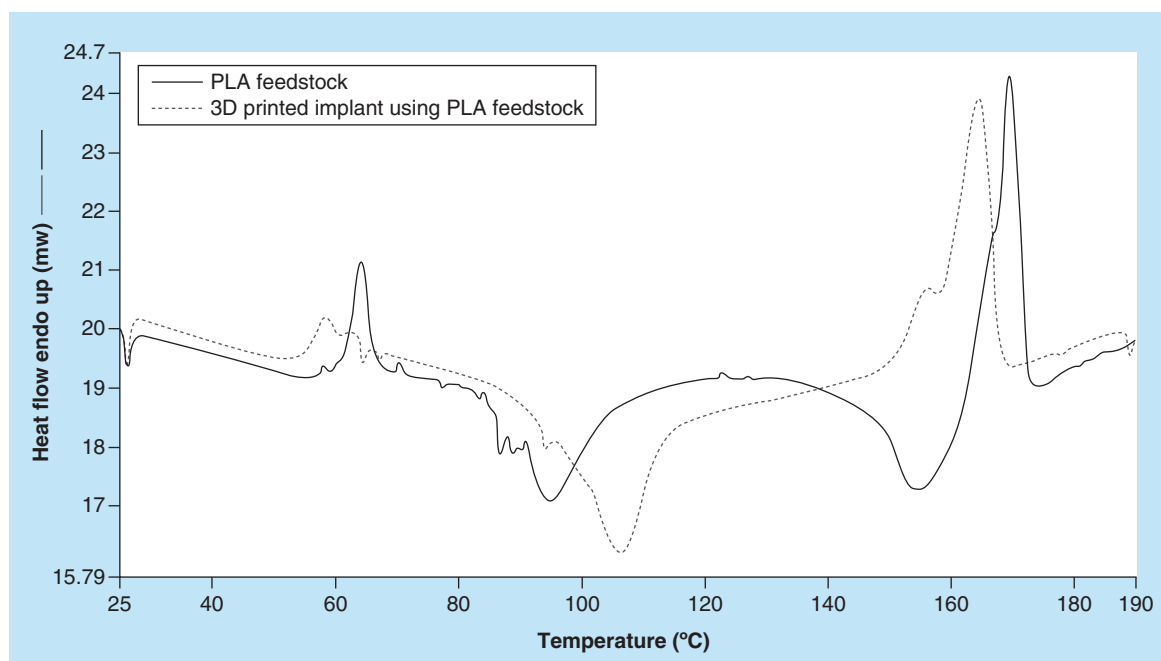


Figure 9. Differential scanning calorimetry plots for polylactic acid feedstock and 3D printed implant using polylactic acid feedstock.

PLA: Polylactic acid.

approach when operating at elevated temperatures at the point-of-care. This is so because the extrusion process typically involves the drug–base blend being exposed to high temperatures for approximately 30 min during translocation along the screw thread.

We believe that the manufacturing conditions would have led to the degradation of the API within this study resulting in the disagreeable drug-containing filament produced and the unpleasant sulfuric odor. Interestingly, not only does the API appear to be affected by the required conditions, the PLA itself has shown a transition from the feedstock material to the extruded material. An alteration in the polymer composition/arrangement could have contributed to this change in behavior and consequently the properties of the PLA. Furthermore, the printing process highlighted modifications to the PLA transition characteristics. The high temperature exposure is consistent between both the extrusion and printing processes therefore it is likely to be the leading factor for these variations. Alongside the manufacturing processes themselves, the API appears to have an impact on the PLA. Here, the key transitions were evident (i.e., the glass transition) along with a possible recrystallization and a melt. However, the extruded PLA being much smoother in terms of its trace could be indicative of the PLA–disulfiram blend being a more crystalline structure.

We conclude, therefore, that there is indeed an interaction between disulfiram and PLA. Further to

this, the enthalpy of crystallization was much lower, 1.632 J/g, when disulfiram was incorporated at 170°C indicating that less energy was required to encourage this recrystallization process. Both the blends were notably more brittle upon handling in contrast to the flexible PLA feedstock. The exemplar study did not report any changes in DSC data upon addition of their API.

Surface energetics assessment

Within this study, the iGC-SEA was applied to determine the surface energetics and surface chemistry (i.e., relative basicity) of the extruded samples produced at 140°C. This study was able to differentiate the differences in surface energetics and surface chemistry (e.g., relative basicity) of the samples. The surface energetics and surface chemistry of materials are known to have important implications in processes involving interfacial interactions such as wetting, coating along with cohesion and adhesion. The data demonstrate that the samples are energetically heterogeneous, meaning the surface energy changes as a function of surface coverage. In addition, it can be clearly observed that the dispersive component contributes a major part of the surface energy. The specific free energies and Gutmann acid/base values indicate that the surfaces of the samples are more basic in nature. This means that the samples possess higher concentrations of electron-donating surface functional groups.

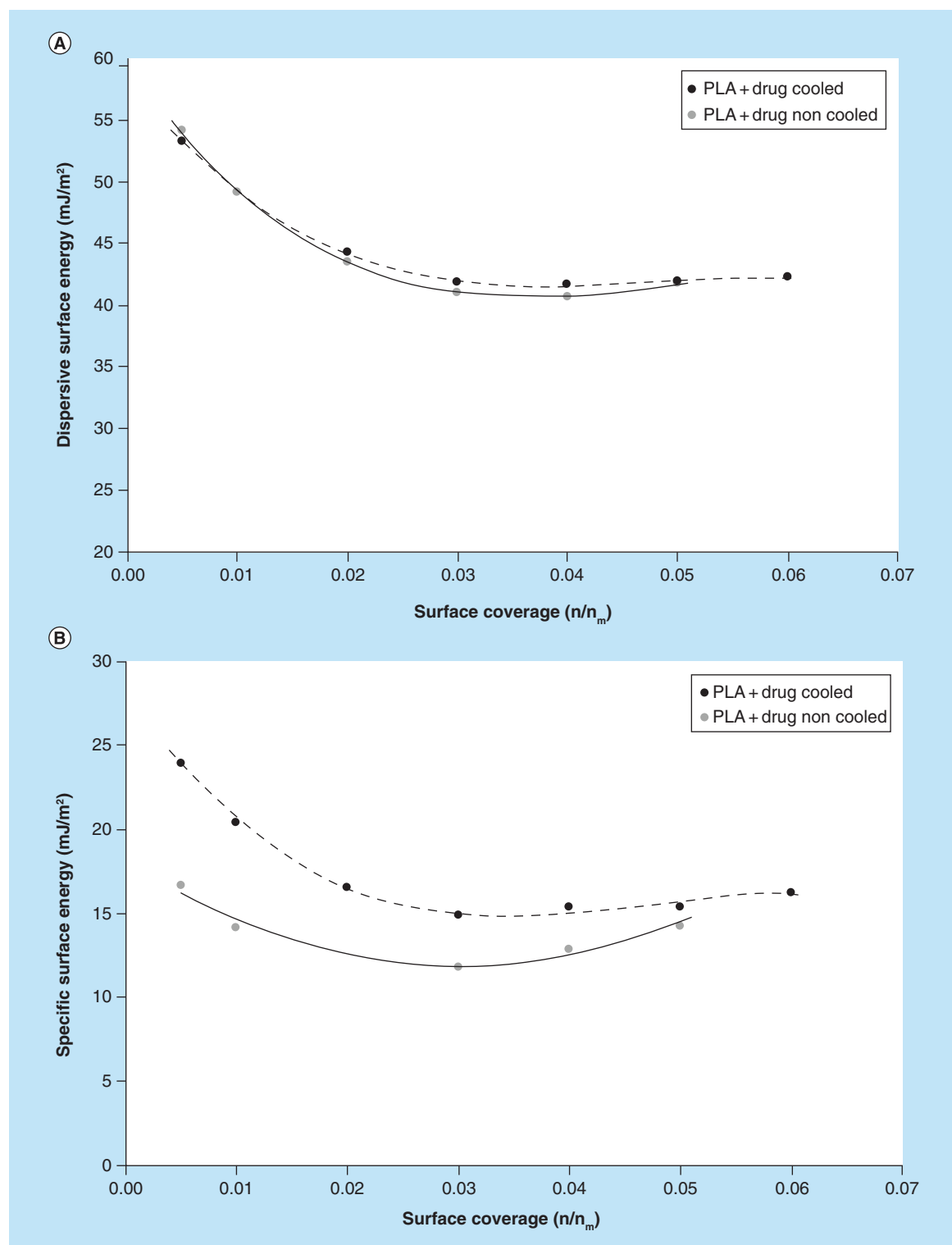


Figure 10. Inverse gas chromatography analysis, as a function of surface coverage, of drug–base combination with thermal history considered. (A) Comparison of the dispersive surface energy profile, as a function of surface coverage. **(B)** Comparison of the specific surface energy profile, as a function of surface coverage. PLA: Polylactic acid.

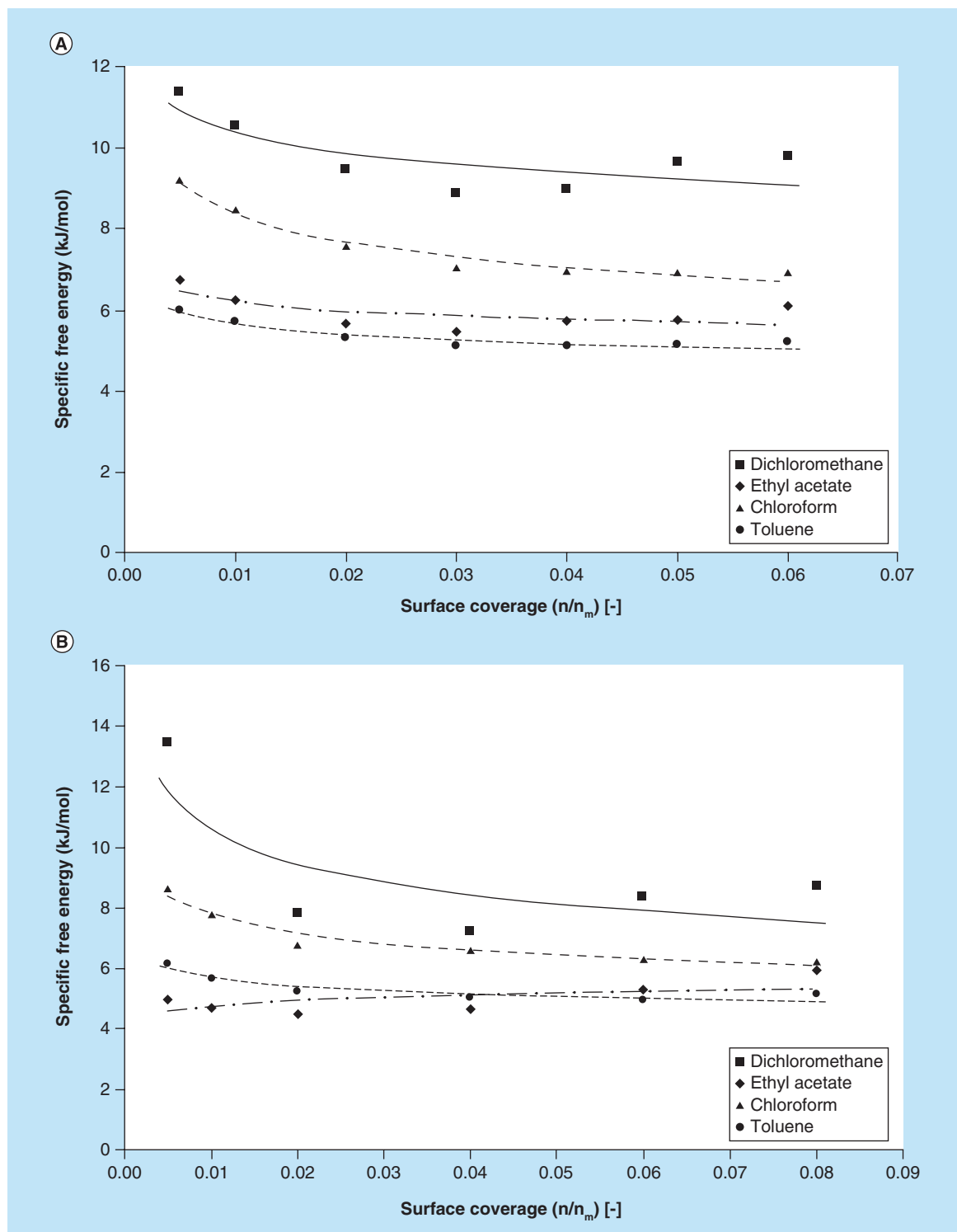


Figure 11. Inverse gas chromatography analysis of drug–base combination with thermal history considered. (A) Specific (acid-base) free energy profiles of different solvents for the polylactic acid + drug cooled sample. **(B)** Specific (acid-base) free energy profiles of different solvents for the polylactic acid + drug noncooled sample. PLA: Polylactic acid.

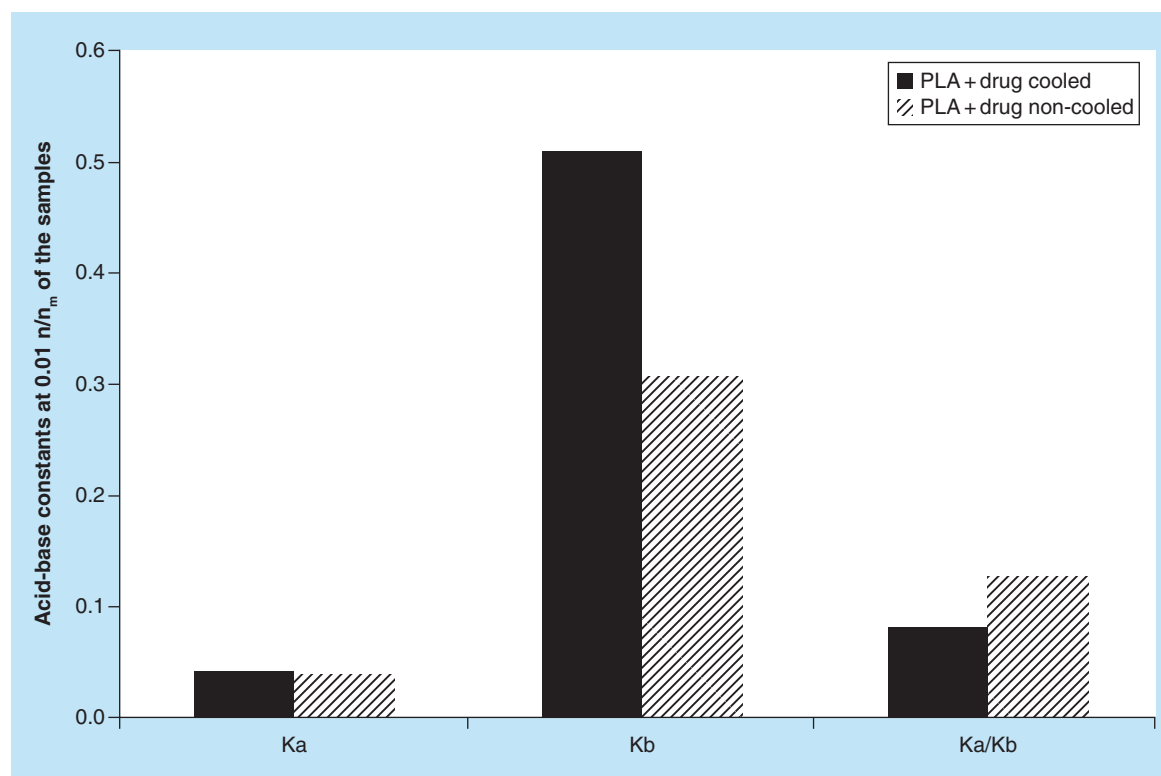


Figure 12. Gutmann acid and base constants of the samples at a certain surface coverage. PLA: Polylactic acid.

Limitations & recommendations

Limitations

The equipment used during this study (e.g., Noztek Pro Extruder & Wanhao 3D Printer) also contributed to the lack of success. As such, when establishing a laboratory space we recommend that the user considers operational tolerances for all pieces of equipment. Ideally, tolerances should be flexible but within range to allow for slight variation in material properties (e.g., feedstock diameter) that will inevitably arise during the preparative stages. In addition, during the manufacture of blend-based pharmaceutical formulations it would seem appropriate to have available a controlled feed to allow the ready addition of the API in a consistent manner plus a recirculation channel to allow effective mixing and minimize material losses. For example, Water and colleagues used a DSM Xplore micro compounder which accommodated 2 min of mixing prior to extrusion [2].

The diameter of the extruder nozzle is a crucial factor to consider for optimal filament generation. Here, the user should ensure that the nozzle is of the appropriate size (e.g., 1.75 mm) such that the resultant filament will match the inlet configuration of the 3D printer head. However, that being said, the viscoelastic nature of the base polymer, and indeed the drug–base blend, should be borne in mind. On release of the

molten material from the nozzle there is potential for the material to swell and bulge [2]. Thus, the resulting variation in the diameter of the feed may be unsuitable for insertion into the 3D printer head. One way in which to circumvent this issue is to modify the operating temperature slightly and in such a way account for polymer swelling on release from the extruder nozzle. Additionally, gravitational forces also influenced the diameter of the extruded filament in this study. As the length of the filament increased the weight pulling on the swollen extrudate also increased and the thinner the strand became. Thus, we advocate the use of a lubricated, plate-like structure in proximity to the nozzle to adequately support the extrudate on release from the nozzle to maintain a consistent diameter.

The 3D printer employed during this study certainly contributed to the difficulties experienced. The high-precision requirement for the filament diameter made the printing process very challenging. If the filament (drug loaded or not) deviated from the diameter of 1.75 mm then the feed system would either not detect its presence or clog. We suggest, therefore, that an adjustable clamp inside this mechanism would be beneficial to allow the feed of filaments that may be for instance of 1.75 ± 0.1 mm. Additionally, improved resolution would provide a smoother, more aesthetically pleasing finish to the dosage forms produced and as

such instills greater patient confidence. This is a prime consideration to take into account ahead of purchasing such a unit. Here, we believe that investment in the most precise 3D printer would certainly be beneficial for the formulator over time.

The greatest limitation to study success was the incompatibility between the base material and API. We believe that base material selection must be determined by considering four key elements; namely the safety profile of the material, manufacturability (including drug–base incompatibilities), drug release characteristics and material degradation over time. As previously stated, PLA is biodegradable and demonstrates a drug release profile covering a number of days, thus making it an ideal material for implantable devices. However, the work presented herein clearly demonstrates that great care must be taken during the manufacturing process.

It is simply not the case to select the base material on one ‘topic,’ a delicate interplay exists between the base material and API of interest. In order to develop current understanding of drug–base incompatibilities it is important to apply a range of advanced materials characterization techniques, including for example DSC and x-ray diffraction. Our observations within the laboratory and data collected in respect of the resultant materials confirm that high operating temperatures have to be carefully considered before manufacture and ideally prescreening of all materials for inclusion in the final formulation must take place prior to manufacture.

Recommendations

We believe that there is a pressing need to investigate alternative base materials, of lower melting temperature, such that the potential of 3D printing may be fully realized when considering personalized medicine paradigms. A prime example is that of PEG, which has a melting range of between 50 and 60°C [26]. However, care must be taken to ensure biocompatibility. This point is acutely illustrated by the warning issued by the US FDA in 2011 regarding PEG 3350 (i.e., Miralax®) and the potential for neuropsychiatric events on ingestion [27].

Similarly, PCL has a lower melting temperature of approximately 60°C with a high thermal stability [28]. This base material has application in the field of tissue engineering via 3D printing as a result of its biocompatible, biodegradable, pore interconnectivity and porosity profile. Furthermore, PCL has reported use in pharmaceutical dosage forms. In 2015, Pathak and coworkers successfully manufactured PCL matrices loaded with doxycycline to be administered via the vaginal route for the treatment of sexually transmitted infections [29]. Thus, PCL could prove to be a suitable excipient for use in drug-eluting constructs in the field

of FDM.

Naturally occurring products may also hold promise as base materials for FDM; examples include stearic acid and oleic acid. Both materials have been successfully applied as support species for hydroxypropyl-methylcellulose-based constructs in 3D printing strategies [30]. Once again, they are of low melting point, namely 70°C and 13–14°C, respectively [31], and therefore have the potential to create a more suitable production environment during the printing process.

Clearly, if the API does degrade during the formulation process then it will no longer hold therapeutic value. Accordingly, if we give consideration to the model API employed within this study, in order to ensure activity on delivery to the body we would require formulation with a biodegradable/biocompatible polymer of significantly lower melting point (e.g., 60°C) as compared with the high operating temperatures noted with PLA. In the same manner, a large number of APIs will experience similar deleterious effects at elevated temperatures, which may be exemplified on consideration of the first-generation antihistamine promethazine that is commonly used as an antiemetic [32]. Hence, we underscore the fact that great attention is needed to establish the suitability of the operating conditions during the 3D manufacturing process. All materials should be taken on their individual merits at the outset and carefully monitored on combination.

Application to healthcare

Despite our study having limited success with regard to producing personalized implantable formulations to manage alcohol misuse, potential undoubtedly exists for the application of 3D printing within the healthcare arena. Here, we have demonstrated that it is imperative to carefully consider the nature of each material in the manufacturing process plus related operating conditions. The 3D printer employed herein was of compact size and therefore ideal for installation and use at the point-of-care. A prime example of this very approach is the personalization of medicine administration within the community pharmacy setting. Clearly, such a strategy would allow for the patient to be considered on an individual basis in terms of their dose requirements and related side effect presentation. Once a patient is electronically logged within the pharmacy system (i.e., correct determination of their patient specific file) then their details can be utilized for efficient and accurate 3D printer dispensing.

Conclusion

This study attempted to manufacture disulfiram-loaded implants via FDM using PLA as the base material. An assessment of the feasibility to utilize these

materials with this method was also carried out. Here, the considerable degradation of disulfiram during the extrusion process and change in PLA characteristics when extruded highlights the considerations that need to be taken for the process to be successful. The high extrusion and printing temperatures required created a number of problems therefore materials with a lower melting point need to be obtained and utilized to allow for printing at temperatures below decomposition values. Moreover, potential interactions between the base material and the API need to be thoroughly investigated prior to manufacturing to avoid any untoward changes in material composition. By utilizing 3D printing there is potential to produce personalized healthcare on a small scale to optimize dosing regimens for patients. Suitable locations for such care would include community pharmacies and outpatient clinics due to their compact size, efficient production and inexpensive nature. Further developments in FDM technology will allow for a more customized approach to modern day healthcare.

Acknowledgements

MJ Davies would like to thank LJMU for funding this research effort. Special thanks go to P Burgess, G Henshaw, N Dempster and R Allen for technical support.

Financial & competing interests disclosure

This research was funded by Liverpool John Moores University. The authors have no other relevant affiliations or financial involvement with any organization or entity with a financial interest in or financial conflict with the subject matter or materials discussed in the manuscript apart from those disclosed.

No writing assistance was utilized in the production of this manuscript

Ethical conduct of research

The authors state that they have obtained appropriate institutional review board approval or have followed the principles outlined in the Declaration of Helsinki for all human or animal experimental investigations. In addition, for investigations involving human subjects, informed consent has been obtained from the participants involved.

Executive summary

- Alcohol misuse is a concern in the developed world and as such a range of treatment options are available.
- Oral regimens rely upon the patient strictly adhering to the prescriber's directions with scope to miss doses if desired, implantable devices circumvent this issue as the drug is constantly delivered under the skin with time.
- Here, we considered the feasibility of loading a base material with disulfiram (which is frequently used in the management of alcohol misuse) and manufacturing 3D implantable devices to satisfy the personalized medicine paradigm.
- During production drug–base incompatibilities were apparent, which precluded effective implant manufacture.
- Thermal analysis confirmed drug–base incompatibilities with the thermal history of the resultant material influencing interfacial acid/base properties.
- A key issue during the manufacturing process was the high temperatures required to melt the base material; the elevated temperatures were not suitable for the material combination in this instance.
- We recommend that base materials of lower melting point are used in the 3D printing process, examples of which include PEG and oleic acid.
- 3D printing holds great promise in the field of personalized, point-of-care disease management. However, careful consideration of drug-base incompatibilities is a must prior to the fabrication of pharmaceutically relevant dosage forms.

References

Papers of special note have been highlighted as:

• of interest; •• of considerable interest

- 1 Alomari M, Mohamed F, Basit A, Gaisford S. Personalised dosing: printing a dose of one's own medicine. *Int. J. Pharm.* 494(2), 568–577 (2015).
- Provides the reader with a summary of the practical and clinical aspects of ink-jet printing that should be reflected upon to enable the technology to become widely recognized in the fields of pharmaceuticals and healthcare.
- 2 Water J, Mohr A, Boetker J, Aho J, Sandler N, Nielsen H, Ratanen J. Three-dimensional printing of drug-eluting implants: preparation of an antimicrobial polylactide feedstock material. *J. Pharm. Sci.* 104, 1099–1107 (2015).
- Successfully produced drug-loaded implantable devices using polylactic acid albeit with a different drug substance. Here, no drug-base incompatibilities were apparent. The paper confirms such an approach is feasible.
- 3 Genina N, Janßen E, Breitenbach A, Breikreutz J, Sandler N. Evaluation of different substrates for inkjet printing of rasagiline mesylate. *Eur. J. Pharm. Biopharm.* 85(3B), 1075–1083 (2013).
- 4 Skowyra J, Pietrzak K, Alhnan M. Fabrication of extended-release patient tailored prednisolone tablets via fused deposition modelling (FDM) 3D printing. *Eur. J. Pharm. Sci.* 68, 11–17 (2015).
- 5 Goyanes A, Wang J, Buazn A, Martinez-Pacheco R, Telford R, Gaisford S, Basit A. 3D printing of medicines: engineering novel oral devices with unique design and drug

- release characteristics. *Mol. Pharm.* 12(11), 4077–4084 (2015).
- **Provides the researcher with a very good overview of the processes underpinning 3D printing within the field of pharmaceuticals.**
- 6 Bardani F. Implant device and dosage form employable therein. European Patent 1216721 A2 (2002).
 - 7 Ventola C. Medical applications for 3D printing: current and projected uses. *P T* 39(10), 704–711 (2014).
 - 8 Schubert C, Langeveld M, Donoso L. Innovations in 3D printing: a 3D overview from optics to organs. *Brit. J. Ophthalmol.* 98(2), 159–161 (2013).
 - 9 Prasada LK, Smytha H. 3D Printing technologies for drug delivery: a review. *Drug Dev. Ind. Pharm.* 42(7), 1019–1031 (2016).
 - 10 Williams J, Adewunmi A, Schek R, Flanagan C, Krebsbach P, Feinberg S, Hollister S, Das S. Bone tissue engineering using polycaprolactone scaffolds fabricated via selective laser sintering. *Biomaterials* 26(23), 4817–4827 (2005).
 - 11 Goyanes A, Buanz A, Hatton G, Gaisford S, Basit A. 3D printing of modified-release aminosalicylate (4-ASA and 5-ASA) tablets. *Eur. J. Pharm. Biopharm.* 89, 157–162 (2015).
 - 12 Storey RA, Ym'en I. *Solid State Characterization of Pharmaceuticals, First Edition*. Blackwell Publishing Ltd, United Kingdom (2011).
 - 13 Alcohol Dependence. www.drinkaware.co.uk/check-the-facts/health-effects-of-alcohol/mental-health/alcohol-dependence
 - 14 Health and Social Care Information Centre. Statistics on alcohol. www.hscic.gov.uk/catalogue/PUB17712/alc-eng-2015-rep.pdf
 - 15 National Institute for Health and Clinical Excellence. Acute withdrawal from alcohol. 2010. www.nice.org.uk/guidance/cg100/ifp/chapter/acute-withdrawal-from-alcohol
 - 16 National Institute on Alcohol Abuse and Alcoholism. Alcohol's effects on the body. www.niaaa.nih.gov/alcohol-health/alphols-effects-body
 - 17 National Institute for Health and Clinical Excellence. Alcohol – problem drinking. <http://cks.nice.org.uk/alcohol-problem-drinking#!scenario:1>
 - 18 BNF 71: British National Formulary 71. British Medical Association & Royal Pharmaceutical Society of Great Britain (2016).
 - 19 Summaries of product characteristics. <https://www.medicines.org.uk/emc/medicine/519/SPC/Antabuse+Tablets++200mg>
 - 20 Summaries of product characteristics. www.medicines.org.uk/emc/medicine/23824/SPC/Nexplanon+68+mg+implant+for+subdermal+use
 - 21 Surface Measurement Systems Limited. London, United Kingdom.
 - 22 Hongbo L, Michel H. Effect of nucleation and plasticization on the crystallization of poly(lactic acid). *Polymer* 48(23), 6855–6866 (2007).
 - 23 Sacui IA, Nieuwendaal RC, Burnett DJ *et al.* Comparison of the properties of cellulose nanocrystals and cellulose nanofibrils isolated from bacteria, tunicate, and wood processed using acid, enzymatic, mechanical, and oxidative methods. *ACS Appl. Mater. Interfaces* 6(9), 6127–6138 (2014).
 - 24 Mittle KL, Pizzi A. *Handbook of Adhesive Technology*. Marcel Dekker Inc., United States of America (2003).
 - 25 Mohammadi-Jam S, Waters KE. Inverse gas chromatography applications: a review. *Adv. Colloid Interface Sci.* 212, 21–44 (2014).
 - 26 The MAK Collection for Occupational Health and Safety 2012. <http://onlinelibrary.wiley.com/doi/10.1002/3527600418.mb2532268kske0010/pdf>
 - 27 U.S Food and Drug Administration 2011. Potential Signals of Serious Risks/New Safety Information Identified by the Adverse Event Reporting System between October – December. (2011). www.fda.gov/Drugs/GuidanceComplianceRegulatoryInformation/Surveillance/AdverseDrugEffects/ucm295585.htm
 - 28 Chia H, Wu B. Recent advances in 3D printing of biomaterials. *J. Biol. Engin.* 9(4), (2015).
 - **Provides a good overview of recent developments in the field of 3D printing.** - 29 Pathak M, Coombe A, Turner M, Palmer C, Wang D, Steadman K. Investigation of polycaprolactone matrices for intravaginal delivery of doxycycline. *J. Pharm. Sci.* 104(12), 4217–4222 (2015).
 - 30 Bayer R, Pyzik A, Allen S. Support materials for 3D printing. WO Patent: 2015108768. (2015).
 - 31 ChemSpider Database. www.chemspider.com/Chemical-Structure.5091.html
 - 32 Chu K, Yalkowsky S. An interesting relationship between drug absorption and melting point. *Int. J. Pharm.* 373(1–2), 24–40 (2009).